LINE-START PERMANENT MAGNET SYNCHRONOUS MOTORS. ANALYSIS AND DESIGN

Dan STOIA[1], Mihai CERNAT[1], Kay HAMEYER[2], Drago BAN[3]

[1]"Transilvania" University of Brasov, Faculty of Electrical Engineering and Computer Sciences
B-dul Eroilor 29, 500036 Brasov, Romania, stoiadan@ymail.com, m.cernat@unitbv.ro

[2]RWTH Aachen University, Institute for Electrical Machines
Schinkelstraße 4, 52062 Aachen, Germany, kay.hameyer@iem.rwth-aachen.de

[3]University of Zagreb, Faculty of Electrical Engineering and Computing
Unska 3, 10000 Zagreb, Croatia, drago.ban@fer.hr

Abstract. The Line-Start Permanent Magnet Synchronous Motor (LSPMSM) attracted a considerable attention because of the higher value of the product between the power factor and the efficiency. The paper proposes an analytical design method for the permanent magnet, considering the operating point on the *B-H* characteristic alias the magnetic flux–magnetomotive characteristic, a design method for the LSPMSM considering the synchronous operation parameters and the asynchronous operation (starting) parameters.
A design example for a motor having rated power 3.5 kW, rated phase voltage 200 V, rated frequency 50 Hz, rated speed 3000 rpm will be presented.

Keywords. AC machines, design, electrical machines, permanent magnet motors, line-start synchronous motor.

1. INTRODUCTION

In the last years, the LSPMSM has received more attention in the academic world and industries [1-38]. Worldwide new legislations demand higher efficiency motors. The use of LSPMM can help to achieve the new requirements. It became competitor to cage induction motor in the general purpose industrial applications due to its high efficiency, high power factor and its ability to self start from the regular fixed frequency supply [5-8].

The structure of LSPMSM is similar to this of the IM but with permanent magnets (PMs) inserted in the rotor [6, 9-11]. The rotor can have many types of configurations since the inserted PMs may have different shapes, materials, sizes and positions [2, 4, 12, 13], which deeply influence the performances of the machine. The line-start property is obtained thanks to the design of the rotor with starting aluminium cage or with solid iron, or with a conducting ring on the surface [5, 14-16].

LSPMSM is in fact a synchronous machine at which the excitation field is produces by permanent magnets instead by a dc field winding. For starting and transients, the machine has the aluminium cage on the rotor.

So, the functioning of the LSPMSM is characterized by two operation modes: the synchronous operation mode at steady state and the asynchronous operation mode at starting and transients [39].

The synchronizing process has been studied in [1-4, 28]. The steady-state characteristics are measured for different values of the output power [18-22].

In general, the LSPMSM has PMs buried below the squirrel-cage and these two constructive parts have different functions under different states.

The PMs operate on alignment torque to drive synchronous speed in steady state and breaking torque in starting period, both dependent of the PM operating point and the non-load emf [9, 18, 19, 23, 35]. So, it is necessary to design PMs considering the alignment and breaking torque at once.

In general, the optimal size of PMs provides the required magnetic flux so that the reactive power exchanged with the power supply is minimal, to get a highest power factor which corresponds to the minimum line current [15].

The rotor cage generates in transient operating modes (starting and load changes) an asynchronous torque.

The breaking torque introduced by PMs in starting period lowers the total torque [11, 32, 34]. Because the PMs are buried below the squirrel cage, magnetic flux barriers in the rotor back iron are necessary. So, additionally to the PM breaking torque, these magnetic flux barriers introduce a breaking reluctance torque because of rotor saliency, which further lowers the total torque in starting period.

In this way, the design of LSPMSM is somehow troublesome because of various line starting performance degrading effects. For the aforementioned reasons, the LSPMSM designer has to find many compromises in the design process between an adequate starting characteristic in the asynchronous operating region and the torque capability and efficiency in the synchronous operating region.

The paper proposes: an analytical design method for the PMs considering the operating point on the *B-H* characteristic taking into account of the iron saturation effect; followed by an analytical design method for the LSPMSM

considering the asynchronous and synchronous behaviour, for operating the motor at steady state near the unity power factor.

2. THE OPERATING POINT OF THE PM WITHOUT ARMATURE REACTION

Neglecting of Magnetic Saturation

Fig. 1 presents the studied LSPMSM. The stator is the same as that of an usual induction motor. The line-start property is obtained thanks to the rotor design, which contains an aluminum cage for asynchronous line starting, two PMs made of NdFeB and two non-magnetic material flux barrier on the quadrature axis to minimize the inter-pole PM leakage flux.

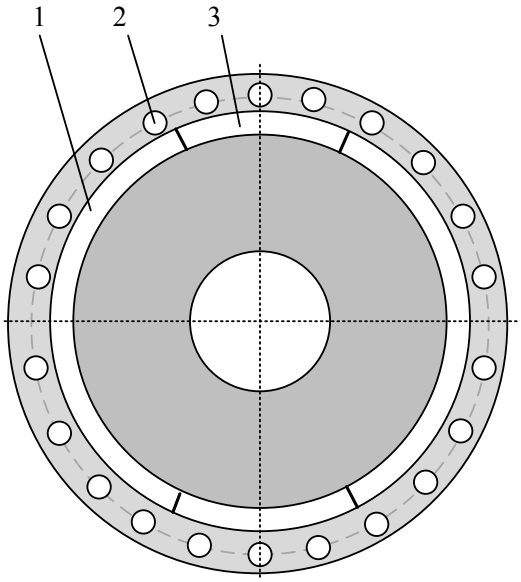

Fig. 1. Cross section of the rotor of a LSPMSM: 1-permanent magnet; 2-cage; 3-non-magnetic flux barrier.

For determining the operating point of the PM used in LSPM motors, the machine is operated as a no load generator. Fig. 2 shows the simplified equivalent circuit of the LSPM machine at no load functioning (without armature field).

In general case, the resultant permeance Λ_t of the external magnetic circuit consists of two components: the useful permeance which is the permeance of the air-gap and the leakage permeance:

$$\Lambda_t = \Lambda_\delta + \Lambda_\sigma = k_{\sigma M}\ \Lambda_\delta \tag{1}$$

The useful permeance Λ_δ corresponds to the useful flux in the active portion of the magnetic circuit. The leakage permeance Λ_σ is the referred leakage permeance of a single PM or of the PM with armature (in rotor and stator slots, the non-magnetic material and the air spaces between the magnet and the laminations steels). The permeances are:

$$\Lambda_M = \frac{\Phi_{rem}}{F_c} = \frac{B_{rem}\ S_M}{H_c\ l_M} = \frac{\mu_0\ \mu_{rec}\ S_M}{l_M} \tag{2a}$$

$$\Lambda_\delta = \frac{\Phi_{\delta 0}}{F_c} = \frac{B_{\delta 0}\ S_\delta}{H_c\ k_C\ \delta} = \frac{\mu_0\ S_\delta}{k_C\ \delta} \tag{2b}$$

$$\frac{\Lambda_M}{\Lambda_\delta} = \mu_{rec}\ k_C \frac{S_M}{S_\delta}\frac{\delta}{l_M} = \mu_{rec}\ k_C \frac{C_\Phi}{C_p} \tag{2c}$$

with the flux concentration factor:

$$C_\Phi = S_M / S_\delta\,. \tag{3}$$

and the permeance coefficient

$$C_p = l_M / \delta \tag{4}$$

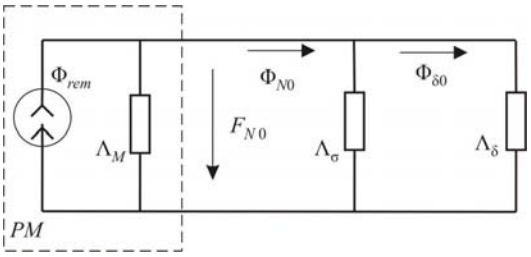

Fig. 2. The equivalent circuit of the LSPM machine without armature reaction.

In Fig. 3 N_0 is the operating point of the PM in the flux-mmf coordinates, which is at the intersection of the linear demagnetizing characteristic of the rare-earth PM (L_{rec}) and the load line (L_{l0}).

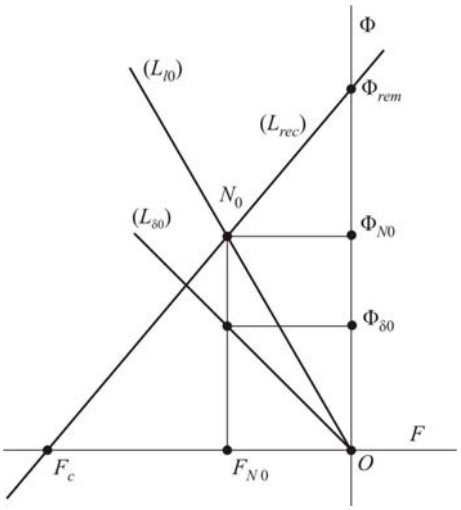

Fig. 3. Determining of the operating point of the PM: Φ_{rem}- remanent flux; F_c – coercive mmf; (L_{rec}) - the recoil line, (L_{l0}) – the load line without armature field; ($L_{\delta 0}$) – the air-gap load line; N_0 – the operating point without armature field.

In Fig. 3, the equations of (L_{rec}), (L_{l0}) and ($L_{\delta 0}$) lines are [40, 41]:

$$\begin{aligned} &(L_{rec}): \quad \Phi = \Phi_{rem} + \Lambda_M\ F; \\ &(L_{l0}): \quad \Phi = -\Lambda_t\ F; \\ &(L_\delta): \quad \Phi = -\Lambda_\delta\ F; \end{aligned} \tag{5}$$

respectively. Consequently, the coordinates of the operating point N_0 are:

$$N_0: \begin{cases} \Phi_{N0} = \Phi_{rem} \dfrac{\Lambda_t}{\Lambda_t + \Lambda_M}; \\ F_{N0} = -\dfrac{\Phi_{rem}}{\Lambda_t + \Lambda_M} \end{cases} \quad (6)$$

and the expression of the air gap flux is:

$$\Phi_{\delta 0} = \frac{\Lambda_\delta}{\Lambda_M + \Lambda_\delta \, k_{\sigma M}} \Phi_{rem} \quad (7)$$

$$k_{\sigma M} = \frac{\Phi_M}{\Phi_{\delta 0}} = \frac{\Lambda_t}{\Lambda_\delta} > 1 \quad (8)$$

The air gap permeance can be expressed as

$$\Lambda_\delta = \frac{\alpha_p \, \tau_p \, l_{FE} \, \mu_0}{2 \, \delta \, k_C} \quad (9)$$

The Carter coefficient $k_C = k_{Cs} \, k_{Cr}$ can be calculated for the stator slots and for the rotor slots separately [13]:

$$k_{Cs} = \left(\frac{t_s}{t_s - \gamma_s \, \delta} \right) \quad (10a)$$

$$\gamma_s = \frac{4}{\pi} \left[\frac{b_{0s}}{2\,\delta} \operatorname{arc\,tg} \frac{b_{0s}}{2\,\delta} - \ln \sqrt{1 + \left(\frac{b_{0s}}{2\,\delta} \right)^2} \right] \quad (10b)$$

The coefficient of the leakage flux can be calculated by [9]:

$$k_{\sigma M} = 1 + \frac{4\, l_M}{\pi \, \mu_{rec} \, \alpha_M \, \tau_p} \ln \left[1 + \frac{\pi \, \delta}{(1 - \alpha_M)\, \tau_p} \right] \quad (11)$$

In this way, by neglecting the magnetic saturation of iron, the air gap flux at no-load operation can be expressed as

$$\Phi_{\delta 0} = \frac{\Phi_{rem}}{k_{\sigma M} + \dfrac{\Lambda_M}{\Lambda_\delta}} = \frac{\Phi_{rem}}{k_{\sigma M} + \mu_{rec} k_C \dfrac{C_\Phi}{C_p}} \quad (12)$$

From the above equation, the expression of the unsaturated flux density on the air-gap results:

$$B_{\delta 0} = \frac{C_\Phi}{k_{\sigma M} + \mu_{rec} \, k_C \dfrac{C_\Phi}{C_p}} B_{rem} \quad (13)$$

The back EMF can be expressed as

$$U_{eM} = 4{,}44 \, f \, w k_w \frac{\Phi_{rem}}{k_{\sigma M} + \mu_{rec} k_C \dfrac{C_\Phi}{C_p}} \quad (14)$$

The permeance coefficient C_p represents the slope of the air-gap line in the second quadrant of the *B-H* plane. This is a measure of the capability of the magnet to withstand demagnetization; a value of the permeance coefficient between 5 and 10 guarantees a successful design. A low value minimizes the magnet cost.

For the sizing procedure of NdFeB PM motors, the air-gap flux density can be initially estimated as $B_{\delta 0} \approx (0.7\text{-}0.9)\, B_{rem}$.

It is note that an increased value of the air-gap flux density can requires wider tooth in order to avoid saturation.

In most electric machine applications, for to get minimum resulting machine volume, the stator tooth width t_s must be half of the stator slot pitch τ_s (i.e. stator slot and tooth widths are equal):

$$t_s = \tau_s / 2 \quad (15)$$

The next task is to determine the pole pitch coverage coefficient α_M and the radial length l_M of the PM for obtaining this structure. The radial length of the magnetic circuit can be expressed as:

$$l_M = \delta \, C_\Phi \, C_P \quad (16)$$

$$C_\Phi = 2 \, \alpha_M / (1 + \alpha_M) = S_M / S_\delta \quad (17)$$

$$S_M = \alpha_M \, \tau_p \, l_{\mathrm{Fe}} \quad (18)$$

The air-gap length δ is usually determined by mechanical constraints and is a given data.

The tooth width t_s is given by

$$t_s = \frac{\pi \, D_i}{k_{\mathrm{Fe}} \, Z_s} \frac{B_{\delta 0}}{B_{sat}} \quad (19)$$

where B_{sat} results from the *B-H* characteristic of the magnetic material.

After inserting $B_{\delta 0}$ from Eq. (13), t_s given by Eq. (19) is a nonlinear function of α_M. Their values can be found iteratively; an initial value for α_M is chosen and the values of air-gap flux density and tooth width are calculated. Condition (15) is checked and the value of α_M is adjusted.

Taking into account of Magnetic Saturation

The expression (12) of the air-gap flux density was deduced considering a linear magnetic circuit. For motors using high-energy PMs it is necessary to consider the nonlinear magnetic characteristics of the steel.

On the other hand, the biggest disadvantages of the NdFeB magnet are the dependence of its remanent flux density with temperature. The temperature coefficient of B_{rem} have negative values (in range of 0.07%-0,13%), thus the accuracy of design can be influenced.

The usual procedure is to add up the mmf drops around the magnetic circuit, taking into account the nonlinear *B-H* curve of the steel and equal their sum to the apparent open-circuit mmf of the PM, which is defined as

$$F_{ca} = l_M \, H_{ca} \quad (20)$$

For a NdFeB PM at room temperature, $H_{ca} = H_c$.

In Fig. 4, the demagnetization curves and their variation with the temperature is presented for PMs made of NdFeB.

The effect of temperature variations on the PM causes the air-gap flux density and the induced back emf to vary.

By proceeding with the individual mmf drops, and starting with the air-gap, the air-gap magnetic flux density is initially assumed to be equal to the value calculated in Eq. (12). Then:

$$F_\delta = k_C \, l_\delta \frac{B_\delta}{\mu_0} \tag{21}$$

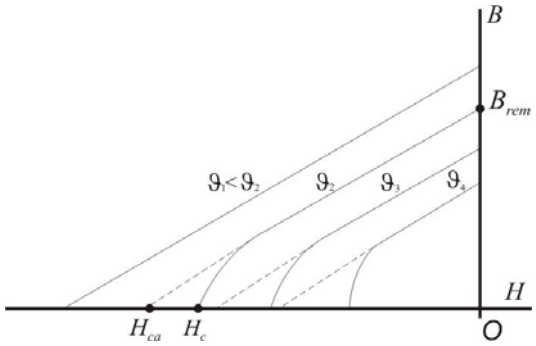

Fig. 4. The demagnetization curves by different temperatures.

Assuming that the stator yoke flux is equal to the air-gap flux crossing over half of the pole area:

$$B_{sy} = B_\delta \frac{S_\delta}{S_{sy}} = \frac{\Phi_\delta}{2\, h_y \, l_{\mathrm{Fe}}} \tag{22a}$$

$$H_y = H_y(B_\delta) \tag{22b}$$

The functional notation represents a linear interpolation along the *B-H* curve of the steel. For this purpose, the *B-H* characteristic of the steel is linearized piecewise and approximated by two line segments (Fig. 5).

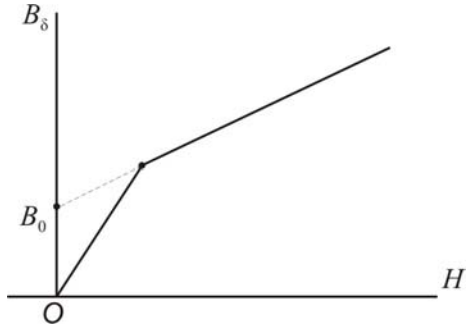

Fig. 5. Piesewise linearized *B-H* characteristic of the PM.

The effect of temperature variations on the PM causes the air-gap flux density and the induced back emf to vary.

The magnetic flux and the magnetic flux density are:

$$\Phi_{N0} = k_{\sigma M} \, \Phi_\delta \tag{23}$$

$$B_{N0} = \frac{B_\delta \, S_\delta}{S_M} k_{\sigma M} = B_\delta \frac{k_{\sigma M}}{C_\Phi} \tag{24}$$

The equation of the demagnetization characteristic is:

$$B_{N0} = \mu_0 \, \mu_{rec} H_{N0} + B_{rem} \tag{25}$$

is used to find H_{N0}, and:

$$F_{N0} = l_M \, H_{N0} \tag{26}$$

Now, all the mmf drops are to add together:

$$F = F_\delta + F_{sy} + F_{st} + F_{rt} + F_{ry} + F_M \tag{27}$$

The principle of iteration is applied. If $F>F_{ca}$, B_δ is decreased and the calculation is repeated. If $F<F_{ca}$, B_δ is increased and the calculation is repeated. These continuous until F is within 0.1% of F_{ca}. An updated value $B_{\delta\, nonlin}$ is obtained. The flux density into the stator and rotor teeth, stator yoke of the machine are computed and will be used to determine the core losses.

The back emf of the machine can be calculated for each speed by using

$$U_{eM} = 4{,}44 \, f \, w k_w \frac{\Phi_{rem}}{k_{\sigma M} + \mu_{rec} k_C k_{sat} \dfrac{C_\Phi}{C_p}} \tag{28}$$

$$k_{sat} = \frac{F_\delta + F_{st} + F_{rt}}{F_\delta} \tag{29}$$

3. THE OPERATING POINT OF THE PM WITH ARMATURE REACTION

Neglecting of Magnetic Saturation

Fig. 6 shows the equivalent circuit of the LSPM machine with armature reaction.

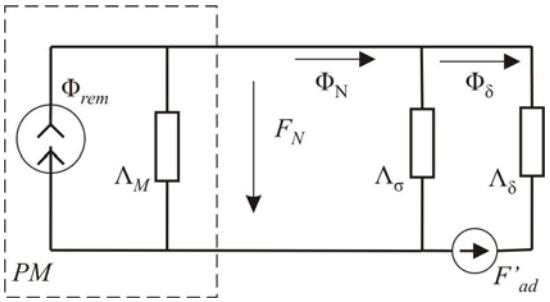

Fig. 6. The equivalent circuit of the LSPM machine with armature reaction.

In Fig. 7 point N is the operating point of the PM in the flux-mmf coordinates, which is at the intersection of the linear demagnetizing linear characteristic of the rare-earth PM and the load line.

In conditions of the armature field action, usually this field demagnetizes the PM, so that the new operating point N is obtained by translation of the N_0 point with the d-axis armature reaction mmf referred to the rotor F'_{ad}. In flux-mmf coordinates, the equations of (L_l) and (L_δ) line are [40, 41]:

$$\begin{aligned} &(L_{rec}): \quad \Phi = \Phi_{rem} + \Lambda_M \, F \\ &(L_l): \quad \Phi = -\Lambda_t \left(F + F'_{ad}\right) \\ &(L_\delta): \quad \Phi = -\Lambda_\delta \left(F + F'_{ad}\right) \end{aligned} \tag{30}$$

respectively.

Consequently, the coordinates of the operating point N in Fig. 2 are

$$\begin{aligned} \Phi_N &= \frac{\Lambda_t \left(\Phi_{rem} - \Lambda_t F'_{ad}\right)}{\Lambda_t + \Lambda_M}, \\ F_N &= -\frac{\Phi_{rem} + \Lambda_M F'_{ad}}{\Lambda_t + \Lambda_M}. \end{aligned} \tag{31}$$

The useful air-gap flux with armature reaction is:

$$\Phi_\delta = \frac{\Lambda_\delta \left(\Phi_{rem} - \Lambda_M F_{ad}^{'}\right)}{\Lambda_M + \Lambda_\delta k_{\sigma M}} \tag{32}$$

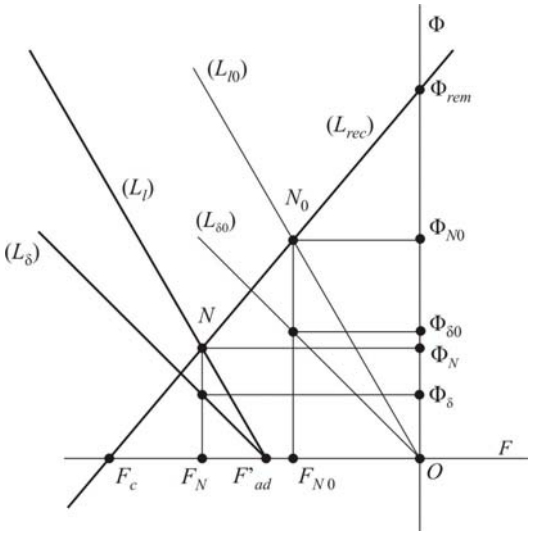

Fig. 7. Determining of the operating point of the PM: Φrem- remanent flux; F_c – coercive mmf; (L_{rec}) – recoil line; (L_{l0}), (L_l) – load line; $(L_{\delta 0})$, (L_δ) – air-gap load line; N_0 – operating point without armature field; N – operating point with armature field.

In this way, by neglecting the magnetic saturation of iron, the air gap flux the at load operation can be expressed as

$$\Phi_\delta = \frac{\Phi_{rem} - \Lambda_M F_{ad}^{'}}{k_{\sigma M} + \dfrac{\Lambda_M}{\Lambda_\delta}} = \frac{\Phi_{rem} - \Lambda_M F_{ad}^{'}}{k_{\sigma M} + \mu_{rec} k_C \dfrac{C_\Phi}{C_p}} \tag{33}$$

From the above equation, the expression of the unsaturated flux density on the air-gap results:

$$B_\delta = \frac{B_{rem}\ C_\Phi - \dfrac{\Lambda_M F_{ad}^{'}}{S_\delta}}{k_{\sigma M} + \mu_{rec} k_C \dfrac{C_\Phi}{C_p}} \tag{34}$$

Thus, the emf by taking into account the armature reaction is defined as

$$U_e = 4{,}44\, f\, w k_w \frac{\Phi_{rem} - \Lambda_M F_{ad}^{'}}{k_{\sigma M} + \mu_{rec} k_C \dfrac{C_\Phi}{C_p}}. \tag{35}$$

The volume of the PM is

$$V_M = \alpha_M\ \tau_p\ l_{\mathrm{Fe}}\ l_M \tag{36}$$

Taking into account of Magnetic Saturation

By taking into account the magnetic saturation of iron, the air gap flux the at load operation can be expressed as:

$$\Phi_\delta = \frac{\Phi_{rem} - \Lambda_M F_{ad}^{'}}{k_{\sigma M} + \dfrac{\Lambda_M}{\Lambda_\delta}} = \frac{\Phi_{rem} - \Lambda_M F_{ad}^{'}}{k_{\sigma M} + \mu_{rec} k_C k_{sat} \dfrac{C_\Phi}{C_p}} \tag{37}$$

From the above equation, the expression of the saturated flux density on the air-gap results:

$$B_\delta = \frac{B_{rem}\ C_\Phi - \dfrac{\Lambda_M F_{ad}^{'}}{S_\delta}}{k_{\sigma M} + \mu_{rec} k_C k_{sat} \dfrac{C_\Phi}{C_p}} \tag{38}$$

Thus, the back emf can be expressed as

$$U_e = 4{,}44\, f\, w k_w \frac{\Phi_{rem} - \Lambda_M F_{ad}^{'}}{k_{\sigma M} + \mu_{rec} k_C k_{sat} \dfrac{C_\Phi}{C_p}}. \tag{39}$$

4. THE STEADY STATE BEHAVIOUR

The voltage equation of LSPM motor is [10, 14, 19, 20]

$$\underline{U} = \underline{U}_{eM} + R\,\underline{I} + \mathrm{j}\left(X_d\ \underline{I}_d + X_q\ \underline{I}_q\right) \tag{40a}$$

$$\underline{U} = \underline{U}_{eM} + R\,\underline{I} + \mathrm{j}\,X_\sigma \underline{I} + \mathrm{j}\left(X_{ad}\ \underline{I}_d + X_{aq}\ \underline{I}_q\right) \tag{40b}$$

Correspondingly, it results the vector diagram presented in Fig. 8.

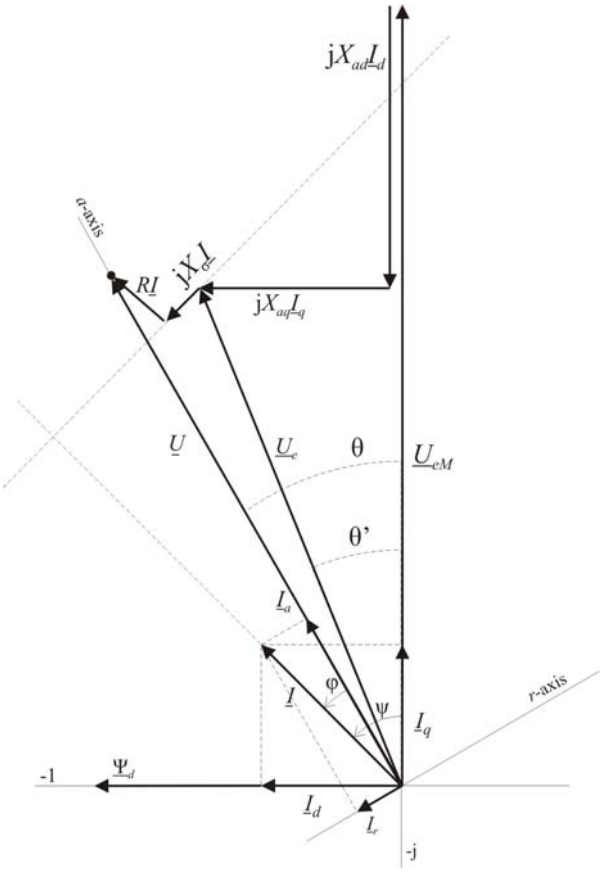

Fig. 8. The vector diagram of the LSPM motor.

$$\underline{U} = \underline{U}_{eM} + \mathrm{j}\,X_\sigma \underline{I} + \underline{I}_d\left(R + \mathrm{j}\,X_{ad}\right) + \underline{I}_q\left(R + \mathrm{j}\,X_{aq}\right) \tag{41a}$$

$$\begin{aligned} \underline{U}_e &= \underline{U} - R\,\underline{I} - \mathrm{j}\,X_\sigma \underline{I} \\ \underline{U}_e &= \underline{U}_{eM} + \mathrm{j}\left(X_{ad}\ \underline{I}_d + X_{aq}\ \underline{I}_q\right) \end{aligned} \tag{41b}$$

$$\begin{aligned} \underline{I} &= \underline{I}_d + \underline{I}_q = \underline{I}_a + \underline{I}_r; \\ I_d &= I\sin\psi; \quad I_q = I\cos\psi \end{aligned} \tag{42}$$

The input voltage projections on the *d*-axis and *q*-axis are:

$$U \sin\theta = I_d\ R + I_q\ X_q \tag{43a}$$

$$U \cos\theta = U_{eM} - I_d\ X_d + I_q\ X_q \tag{43b}$$

The components of the current are

$$I_d = \frac{U\ (X_q \cos\theta - R \sin\theta) - U_{eM}\ X_q}{X_d\ X_q + R^2} \tag{44a}$$

$$I_q = \frac{U\ (R \cos\theta + X_d \sin\theta) - U_{eM}\ R}{X_d\ X_q + R^2} \tag{44b}$$

are obtained by solving Eqs. (4)

As it can be seen in Eq. (2), the vector of the input current I can be decompose in two other components, namely the active component I_a and the reactive component I_r. But

$$I = \frac{P_{em}}{\sqrt{3}\,U} = \sqrt{I_a^2 + I_r^2} = \sqrt{I_d^2 + I_q^2} \tag{45}$$

Using Eqs. (44) on obtain:

$$I = \frac{U}{X_d X_q + R^2} \times \\ \times \left[(X_q \cos\theta - R \sin\theta - U_{eM} X_q)^2 + \right. \\ \left. + (R \cos\theta + X_d \sin\theta - U_{eM} R)^2 \right]^{1/2} \tag{46}$$

and by neglecting the armature resistance and the leakage reactance, the components Ia and Ir of the input current are

$$I_a = \left[\frac{U_{eM}}{X_{ad}} - \frac{U}{X_{ad}} \left(1 - \frac{X_{ad}}{X_{aq}} \right) \cos\theta \right] \sin\theta \tag{47a}$$

$$I_r = -\left[\frac{U}{X_{ad}} - \frac{U_{eM}}{X_{ad}} - \frac{U}{X_{ad}} \left(1 - \frac{X_{ad}}{X_{aq}} \right) \cos\theta \right] \cos\theta \tag{47b}$$

Any change in the input voltage at T_l=0 or T_l=const results in a change in the armature current and power factor.

The V curve at no-load operation

The loci of the armature current with increaseing the armature voltage are the Mordey's V curve of the PM motor (Fig. 9).

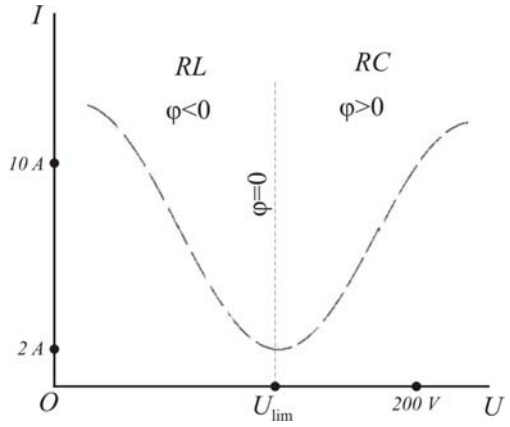

Fig. 9. V curve of the LSPMSM at no-load operation.

For operating the machine at unity power factor, the arma ture voltage $U_{\lim}$ corresponding to the operating point of the V curve where the current is smallest, where the LSPMSM uses neither field weakening nor field strengthening is expressed as:

$$U_{\lim} = \sqrt{U_{eM}^2 + (X_m\ I)^2} \tag{48}$$

$$X_m = 2\ X_{ad}\ X_{aq} / \left(X_{ad} + X_{aq} \right) \tag{49}$$

In this mode of operation, the input current is slightly leading.

The electromagnetic torque

The phasor diagram can also be used to find the input power, i.e:

$$P_{in} = 3\,U\ I \cos\varphi = 3\,U\ (I_q \cos\theta - I_d \sin\theta) \tag{50}$$

From Eqs. (4) and Eq. (11) it results

$$P_{in} = 3\,[U_{eM}\ I_q + RI^2 + I_d\ I_q (X_d - X_q)] \tag{51}$$

Because the stator cote less has been neglected, the electromagnetic power is the motor input power minus the stator winding losses:

$$\Delta P_w = 3\ R\ I^2 = 3\ R\ (I_d^2 + I_q^2) \tag{52}$$

$$P_{em} = P_{in} - \Delta P_w = 3\,[U_{eM}\ I_q - I_d\ I_q (X_q - X_d)] \tag{53}$$

The electromagnetic torque developed by a salient-pole synchronous motor, by neglecting the armature resistance is:

$$T_{em} = \frac{P_{em}}{2\,\pi\,n_s} = \\ = \frac{3}{2\,\pi\,n_s} \left[\frac{U\ U_{eM}}{X_d} \sin\theta + \frac{U^2}{2} \left(\frac{1}{X_q} - \frac{1}{X_d} \right) \sin 2\theta \right] \tag{54}$$

which can be expressed also as:

$$T_{em} = \frac{3\,U_{eM} I}{\Omega} \cos\psi + \frac{3}{2\,\Omega} \left(X_d - X_q \right) I^2 \sin 2\psi \tag{55}$$

From Eqs. (19) and (20) it can be seen that the electromagnetic torque is in direct proportion to the back emf.

The emf is in direct proportion to the magnetic remanence of the PM. So, due to the temperature effect on the magnetic material, the emf can have different values. By decreasing of the remanence of PM, the value of the breaking torque will decrease too.

In Eq. (19), the angular synchronous speed

$$\Omega_s = 2\,\pi\,n_s \tag{56}$$

is equal to the mechanical angular speed of the rotor. In a PM salient-pole synchronous motor, the electromagnetic torque has two components (Fig. 4):

$$T_{em} = T_{syn} + T_{rel} \tag{57}$$

$$T_{syn} = \frac{3}{2\,\pi\,n_s} \frac{U\ U_{eM}}{X_d} \sin\theta \tag{58}$$

$$T_{rel} = = \frac{3}{2\,\pi\,n_s} \frac{U^2}{2} \left(\frac{1}{X_q} - \frac{1}{X_d} \right) \sin 2\theta \tag{59}$$

From Eqs. (25)-(26) it can be seen that the synchronous

torque T_{syn} is a function of both input voltage and no-load emf, while, the reluctance torque T_{rel} depends only of the input voltage U.

The effect of the temperature growing on the maximum value of the electromagnetic torque i.e. pull-out torque is obtained in order to simplify the equation. Let

$$A = \frac{3\ p\ U}{2\ \pi\ n_s\ X_d}; \quad k = \frac{U}{2}\left(1 - \frac{X_d}{X_q}\right) \qquad (60a, b)$$

So, the electromagnetic torque is

$$T_{em} = A\,U_{eM}\sin\theta - k\ A\sin 2\theta \qquad (61)$$

and the pull-out torque can be expressed as:

$$T_{p.o.} = \frac{A\sqrt{3k^2 + 2U_{eM}\sqrt{2U_{eM}^2 + 3k^2 - 2U_{eM}}}}{3k} \times \times\left(3\,U_{eM} + \sqrt{U_{eM}^2 + 3k^2}\right) \qquad (62)$$

Fig. 10 presents the pull-out torque as a temperature growing function.

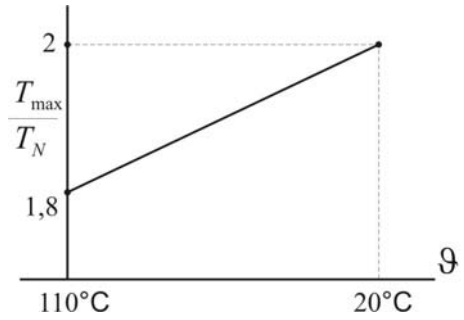

Fig. 10. The pull-out torque as a temperature growing function.

Analysis of the Steady State of the Designed LSPMSM

The design input data are shown in Tab. 1. The specifications of the chosen permanent magnet are shown in Tab. 2

Tab. 1. The input data of the designed LSPMSM.

Rated active power [kW]	P_N	3.5
Rated phase voltage, rms value [V]	U_N	200
Rated frequency [Hz]	f_N	50
Synchronous speed [rpm]	n_s	3000

Ferromagnetic material used in stator and rotor back irons is chosen based on their losses at working point and saturation level. From the *B-H* characteristic, the saturated magnetic flux density B_{sat}=1.8 T (at 50 Hz) results. The stacking factor of the magnetic circuit is α_{stack}=0.94.

Tab. 3 shows the numerical values of the parameters of the designed LSPMSM, relevant for the steady state operating mode.

Tab. 2. The permanent magnet specifications

Permanent magnet type	MQ3G32SH	
Remanent flux density [T]	B_{rem}	1.16
Coercive magnetic field intensity [kA/m]	H_c	828
Magnetic energy density [kJ/m^3]	$(BH)_{\max}$	239
Recoil relative permittivity	μ_{rec}	1.05
Temperature coefficient of remanent flux density [°C^{-1}]	α_B	-0.1%

Tab. 3. The parameters of the designed LSPMSM, relevant for the steady state operating mode.

The voltage corresponding to the minimum of the current on the Mordey's V curve, rms value, rms value [V]	$U_{\lim}$	135
Rated current, rms value [A]	I_N	10
Stator resistance [Ω]	R	0.675
Stator leakage reactance [Ω]	X_σ	0.278
Magnetizing reactance [Ω]	X_d	5
d-axis synchronous reactance [Ω]	X_q	5.05
q- axis synchronous reactance [Ω]	X_m	5.6
Saliency ratio	ξ	1.1

With these parameters, by applying Eqs. (12), (13) on obtain the Mordey's V curve at no-load operation. From the V curve of the designed motor at no-load and at power unit factor, the value of $U_{\lim}$ can be obtained.

The computed values of the steady state main parameters are:

$T_{em\ \max}$=31.74 Nm,
$T_{em\ n}$ =11 Nm,
$I_{\max}$=17.8 A;
θ_{n0}=20°;
$\theta_{\lim}$=98°;
cos φ=0.992.

Fig. 11 shows the torque-angle characteristic of the designed motor.

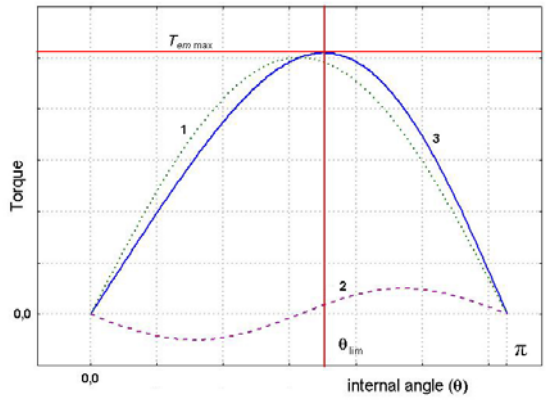

Fig. 11. The synchronous torque and the reluctance torque of the designed LSPMSM.

5. THE STARTING BEHAVIOUR

The equations of LSPM motor can be deduced from the general equations of the Blondel dynamic model. So, in *d*-axis the following set of equations is valid [9, 10, 39]:

$$\begin{aligned} u_d &= R_d\ i_d + \mathrm{p}\,\Psi_d; \\ u_q &= R_q\ i_q + \mathrm{p}\,\Psi q; \\ 0 &= i'_{Dd} R'_{Dd} / s + \mathrm{p}\,\Psi_{Dd}; \\ 0 &= i'_{Dq} R'_{Dq} / s + \mathrm{p}\,\Psi_{Dq}. \end{aligned} \tag{63}$$

The linkage fluxes in the above equations are defined by:

$$\begin{aligned} \Psi_d - \Psi_{Md} &= \left(L_{ad} + L_\sigma\right) i_d + L_{ad}\ i'_{Dd} = \\ &= L_d\ i_d + L_{ad}\ i'_{Dd} \\ \Psi_q &= \left(L_{aq} + L_\sigma\right) i_d + L_{aq}\ i'_{Dq} = L_q\ i_q + L_{aq}\ i'_{Dq} \\ \Psi_{Dd} - \Psi_{Md} &= L_{ad}\ i_d + \left(L_{ad} + L'_{Dd}\right) i'_{Dd} \\ \Psi_{Dq} &= L_{aq}\ i_q + \left(L_{aq} + L'_{Dq}\right) i'_{Dq} \end{aligned} \tag{64}$$

From the above equations on obtain

$$\begin{aligned} \Psi_d - \Psi_{Md} &= \left(L_d - \frac{\mathrm{p}\ L_{ad}^2}{R'_{Dd} / s + \mathrm{p}\ L'_{Dd}} \right) i_d = L_{dp}\ i_d \\ \Psi_q &= \left(L_q - \frac{\mathrm{p}\ L_{aq}^2}{R'_{Dq} / s + \mathrm{p}\ L'_{Dq}} \right) i_q = L_{qp}\ i_q \end{aligned} \tag{65}$$

with the operator $\mathrm{p} = \mathrm{j}\, s\, \omega_s$.

The operational impedances Z_{dp} and Z_{qp} of the LSPM motor, related to the power source are defined as [25]

$$Z_{dp} = R + \omega_s L_{dp}; \qquad Z_{qp} = R + \omega_s L_{qp} \tag{66}$$

The input equivalent impedance is [10]:

$$\underline{Z}_{in} = R + \mathrm{j}\ X_\sigma + \frac{\left(R'_D / s + \mathrm{j}\ X'_{D\sigma}\right) \mathrm{j}\ X_m}{R'_D / s + \mathrm{j}\ X'_{D\sigma} + \mathrm{j}\ X_m} \tag{67}$$

In general, into the equation of the torque there are three components: the non vibratory torque (effective torque), which does not change with time, the first vibratory torque, which changes with time and slip frequency $f_s = s f$ and the second vibratory torque, which changes with time and the double slip frequency. During asynchronous operation, the rotating field passes on the magnet poles with the speed.

$$n = \left(1 - s\right) \frac{60\ f_s}{p} \tag{68}$$

The breaking torque

The "synchronous part" of the LSPM machine sees the supplying network as a terminal short-circuit because of low values of the operational reactance at low frequency $s\omega_s$. In these conditions, the breaking torque will be associated with the stator copper losses because of the current induced by the PMs [4]:

$$I_k = U_{eM} \frac{\left(1 - s\right) \sqrt{\left(1 - s\right)^2 X_q^2 + R^2}}{\left(1 - s\right)^2 X_d\ X_q + R^2} \tag{69}$$

The active power generated by the short-circuit current is

$$P_k = 3\ R\ I_k^2 \tag{70}$$

By introducing the notations

$$\xi = X_q / X_d \tag{71}$$

$$\zeta = R / X_q \tag{72}$$

the power expressed by Eq. (70) produces the breaking torque:

$$T_{M\,br} = -\frac{3p}{2} \frac{\left(1 - s\right) U_{eM}^2}{\omega_s} \frac{\zeta}{X_q} \frac{\left(1 - s\right)^2 + \zeta^2}{\left[\left(1 - s\right)^2 / \xi + \zeta^2\right]^2} \tag{73}$$

The slip value for obtaining the maximum breaking torque:

$$s_k = 1 - \zeta \sqrt{\frac{3}{2}\left(\xi - 1\right) + \sqrt{\frac{3}{2}\left(\xi - 1\right)^2 + \xi}}\ . \tag{74}$$

From Eq. (73) it can be seen that the PM braking torque is in direct proportion to the square of emf, which can be expressed as in Eq. (28).

The cage torque

The expression for the cage torque can be written as [3]:

$$T_c = \frac{3p}{2} \frac{U^2\ X_m^2}{\omega_s} \frac{s\ R'_D}{a_1 + b_1 s + c_1 s^2} \tag{75}$$

$$\begin{aligned} a_1 &= R_D'^{\,2} \left[R^2 + \left(X_{\sigma 1} + X_m\right)^2 \right]; \\ b_1 &= 2\ R\ R'_D\ X_m^2; \\ c_1 &= \left(X_\sigma\ X_m + X'_{D\sigma}\ X_m + X_\sigma\ X'_{D\sigma}\right)^2 + \\ &\quad + R^2 \left(X_{\sigma 1} + X_m\right)^2. \end{aligned} \tag{76a, b}$$

$$R'_D = R'_{Dd} = R'_{Dq}; \quad X'_{D\sigma} = X'_{D\sigma d} = X'_{D\sigma q}. \tag{77}$$

The electric speed at which the asynchronous torque is maxim is given by [3]:

$$\omega_c = s_k\ \omega_s = \omega_s \sqrt{a_1 / c_1} \tag{78}$$

In starting process, the squirrel cage is one key point. The design of the squirrel cage mainly contains the dimension design and the number selection of rotor slots. In a LSMPMSM, the squirrel cage is only functional when the rotor is starting up. Therefore, the design of the squirrel cage mainly focused on a good starting ability. While the cage resistance is relatively high, the motor will produce high starting torques even under low starting current. While the cage resistance is relatively low, the synchronizing capability is better but the starting current is higher. Pyriform slots with flat bottom are in general used on the rotor core for the purpose of reducing the leakage coefficient.

Due to the skin effect, at the beginning of starting, the rotor resistance will increase and the leakage equivalent resistance will decrease. In these conditions, the starting performances will be greatly improved. During the starting process, the average torque have two components, i.e. the braking torque and the cage torque:

$$T_{av} = T_{Mbr} + T_c \tag{79}$$

The slope of the damped oscillations near to the end of the starting process, is identified as [3]:

$$D = \frac{p}{2\,\omega_s\, s}\left(T_c - T_{M\,br} - T_l\right) \tag{80}$$

In starting process, the variety of armature current can be approximately divided into four stages.

Stage one: *accelerating process*. The rotor accelerates from standstill. Due to the low speed, the slip is close to 1, the armature current is high and the electromagnetic torque is also high, thus the rotor runs with high acceleration.

Stage two: *approaching synchronizing process*. The speed rises continuously, and the slip is close to zero, but acceleration becomes lower and the armature current decreases significantly.

Stage three: *pulling into synchronization period*. The motor goes into the damped oscillation procedure.

Stage four: *synchronous operation period*. The waveforms of the armature current tend towards stabilization after several oscillations.

For the purpose of obtaining a higher value of the product between the power factor and the efficiency under load operation, the main value of input voltage must be lower than its rated value (135 V versus 200 V). For the design purpose, the cage resistance is relatively high and the motor will produce high-starting torque even under low starting current. However, increasing the rotor resistance has a beneficial effect on the early start. On the other hand, the higher rotor resistance means that the slope of the asynchronous torque near the synchronous speed is very low. Due to the presence of the magnet braking torque, which is proportional to the square of the no-load voltage, the effective slope or the damping constant D has a value that is much dependent on the no-load voltage.

An increase of the no-load voltage can lead to a reduced critical load torque. An optimum can be found for the no-load voltage to maximize the critical load torque. Note that the decreasing of the volume of the PMs gives a better synchronization capability of motor with high power factor.

On the other hand, the value of the back emf of the PM affects the value of the reactance X_m: increasing the amount of magnets increases the no-load voltage and decreases the magnetizing reactance. Therefore, by increasing the volume of magnet on obtain a better synchronization capability but a lower critical load torque.

Analysis of the Starting Process of the Designed LSPM Machine

Tab. 4 shows the numerical values of the parameters of the designed LSPM machine, relevant for the starting operation.

From the V curve at no-load operation, the armature voltage $U_{\lim}$ corresponding to the operating point of the V curve where the current is smallest, where the LSPMSM uses neither field weakening nor field strengthening is deduced from Fig. 9 and the no-load emf is calculated by Eq. (81).

Tab. 4. The parameters of the designed LSPM machine, relevant for the starting operating mode

No-load emf (without armature reaction), rms value [V]	U_{eM}	130
Stator resistance [Ω]	$R_d = R_q = R$	0.675
Cage (damper) resistance [Ω]	$R'_{Dd} = R'_{Dq} = R'_D$	0.675
Stator leakage reactance [Ω]	$X_{\sigma d} = X_{\sigma q} = X_\sigma$	0.278
Cage leakage reactance [Ω]	$X'_{D\sigma d} = X'_{D\sigma q} = X'_{D\sigma}$	0.237
Magnetizing reactance [Ω]	X_m	5
Saliency ratio	ξ	1.1
Number of stator slots	Z_s	30
Number of rotor slots	Z_r	22
Lamination stack length [mm]	l_{Fe}	90
PM length [mm]	l_M	6
Mean PM diameter [mm]	D_M	90
Air-gap length [mm]	δ	0.8
Pole pitch coverage coefficient of the PM	α_M	0.85

The condition of a good starting capability with a high value of the product between the power factor and the efficiency at load operation is [2]:

$$U_{eM} \cong 0.93\, U_{\lim} \tag{81}$$

During the acceleration time interval of the starting process, the slip is high (from 1 to 0.6), the frequency of the rotor current is also high, the average cage torque is positive and contributes to rotor acceleration, while the average PM torque is negative and acts as a brake.

For the chosen architecture of the LSPMSM, the saliency is very low (ξ=1.1) and consequently the reluctance component of the braking torque is very low too.
The armature current I, the induced current I_k, the input impedance and the components of the torque have the values indicated in Tab. 5 and Tab. 6.

Tab. 5. Values of functioning parameters for $s \in [0.6, 1]$

s	I [A]	I_k [A]	T_c [Nm]	T_b [Nm]	Z_p [Ω]
1	58	0	24.0	O	0.734
0.9	57	14.0	24.0	-3.15	0.740
0.8	53	17.5	23.5	-6.00	0.742
0.7	51	18.5	22.0	-5.00	0.750
0.6	43	20.0	20.0	-4.00	0.756

When the slip value becomes less than $s = 0.6$, the pull-in effect of the synchronization occurs, acceleration becomes lower and correspondingly the armature current decreases rapidly (Tab. 5).
When the slip value becomes less than $s = 0.3$, the motor goes into the damped oscillations (Tab. 6). When the slip is less than $s = 0.25$ the value of the input impedance becomes very high $Z_p = 20\ \Omega$, and the rotor is accelerated up to the synchronous speed, mainly by the PM torque.

Tab. 6. Values of functioning parameters for $s \in [0.3, 0.5]$

S	I [A]	I_k [A]	T_c [Nm]	T_b [Nm]	Z_p [Ω]
0.5	25	19.5	18.2	-2.5	0.78
0.4	23	19.5	16.5	-2.1	0.81
0.3	20	19.7	14.5	-2	0.82

When the slip is less than $s = 0.3$ the value of the input, impedance becomes very high $Z_p = 20\ \Omega$, and the rotor is accelerated up to the synchronous speed, mainly by the PM torque.

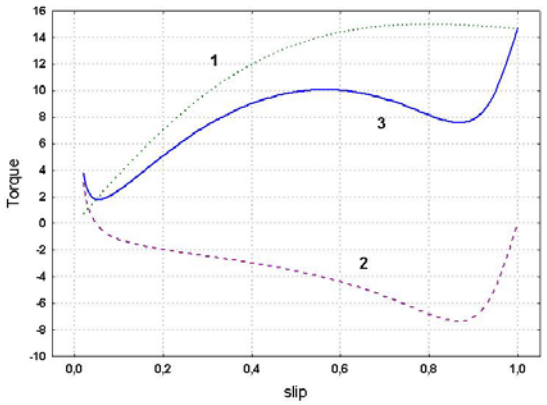

Fig. 12. Cage torque (1), braking torque (2) and average torque (3) of the designed LSPMSM.

At $s = -0.2$ the value of the PM torque is $T_{PM} = 5$ Nm. The cage torque becomes oscillating with a zero mean value. After the synchronization, the cage torque and the braking torque approach small values but not zero

The induced current is $I_k = 20$ A, the PM torque is $T_{PM} = 1.25$ Nm, and the cage torque is $T_r = 0.3$ Nm because the *d*- and *q*-axes reactances are about the same value.

6. CONCLUSION

In this paper a grapho-analytical method for the size up procedure of PMs used in LSPMSM is proposed. Using this theoretical approach the amount of magnet for the required dynamic and steady state performances of this motor can be calculated. The designed operating point of the PM offers the advantage of a large magnetic energy density, near of its maximum.

Then an analytical design method for the LSPMSM considering the synchronous operation parameters is proposed. Using this theoretical approach, the steady state characteristics and the synchronous (alignment) torque were been calculate. In the design process, the LSPM designer has to find the compromise between an adequate starting characteristic in the asynchronous operating region and the torque capability and power factor × efficiency product in the motor's synchronous operating region.

Then an analytical design method for the LSPMSM considering the asynchronous starting parameters (voltage, emf and equivalent resistance of the rotor cage) is proposed.

The LSPM designer has to find many compromises in the design process:

- the compromise between the value of starting torque, which depends mainly on the squirrel-cage design and material, and the starting current;
- the compromise between the value of braking torques (due to the presence of PMs in the asynchronous operating region) which depends mainly on the placement, dimensions and the value of energy product of PMs, which has the principal effect on the motor's synchronization capability;
- the compromise between an adequate starting characteristic in the asynchronous operating region and the torque capability and the product power factor × efficiency in the synchronous operating region.

7. REFERENCES

[1] C.A. da Silva, J. Cardoso, and R. Carlson, "Analysis of a Three-Phase LSPMM by Numerical Method," *IEEE Trans. Magnetics*, Vol. 45, No. 3, March 2009, pp.1792-1795.

[2] F. Libert, J. Soulard, and J. Engstrom, "Design of a 4-pole line start permanent magnet synchronous motor," *Proc. ICEM* 2002, Brugge, Belgium, Aug. 2002.

[3] J. Soulard and H.P. Nee, "Study of the synchronization of line-start permanent magnet synchronous motors," *Proc. of* 2000 *IEEE Ind. Appl. Conf.*, Roma, 8-12 Oct. 2000, vol. 1, pp. 424–431.

[4] K. Kurihara and A. Rahman, "High-efficiency line-start interior permanent-magnet synchronous motors," *IEEE Trans. Ind. Appl.*, vol. 40, no. 3, May/Jun. 2004, pp.789–796..

[5] E. Peralta-Sanchez and A.C. Smith, "Line-start permanent-magnet machines using a canned rotor," *Proc. IEMDC* 2007, 3-5 May 2007, vol. 2, pp. 1084–1089.

[6] J. Salo, T. Heikkila, J. Pyrhonen, "New low-speed high-torque permanent magnet synchronous machine with buried magnets," *Proc. ICEM* 2000, 28-30 August, 2000, Espoo, Finland, vol.2, pp.1246-1250.

[7] A. Abbas, H.A. Yousef, O.A. Sebakhy, "FE Parameters Sensitivity Analysis of an Industrial LS Interior PM Synchronous Motor," *IEEE Power and Energy Society General Meeting – Conversion and Delivery of Electrical Energy in the* 21*st Century*, 20-24 July 2008 pp.1-6.

[8] T. Ding, N. Takorabet, F.M. Sargos, and X. Wang, "Design and Analysis of Different Line-Start PM Synchronous Motors for Oil-Pump Applications," *IEEE Trans. Magnetics*, Vol. 45, No. 3, March 2009, pp. 1816-1819.

[9] V.B. Honsinger, "Permanent Magnet Machines: Asynchronous Operation," *IEEE Trans. Power Apparatus and Systems*, Vol. PAS-99, No. 4 July/Aug 1980, pp. 1503-1509.

[10] J.F. Gieras, M. Wing, "Permanent magnet motor technology," Marcel Dekker Inc. New York, 2002.

[11] M. Rahman, A. Osheiba, T. Radwan, "Synchronization process of line-start permanent magnet synchronous motor," *Electric Machines and Power Systems*, vol. 25, 1997, pp 577-592.

[12] Q.F. Lu and Y.Y. Ye, "Design and Analysis of Large

Capacity Line-Start Permanent-Magnet Motor," *IEEE Trans. Magnetics*, Vol. 44, No. 11, Nov. 2008, pp 4417-4420.

[13] W.H. Kim, K.C. Kim, S.J. Kim, et al., "A Study on the Optimal Rotor Design of LSPM Considering the Starting Torque and Efficiency," *IEEE Trans. Magnetics*, Vol. 45, No. 3, March 2009, pp. 1808-1811.

[14] A.M. Knight and C.I. McClay, "The design of high-efficiency line start motors," *IEEE Trans. Ind. Appl.*, vol. 36, no. 6, Nov./Dec. 2000, pp. 1555–1562,.

[15] D. Rodger, H.C. Lai, R.J. Hill-Cottingham, P.C. Coles and F. Robinson, "A new high efficiency line start motor with high starting torque," *Proc. Int. Conf. PEMD* 2006, 4-6 April 2006, pp. 551–555.

[16] L. Weili, Z. Xiaochen, C. Shukang, C. Junci, "Study of Solid Rotor Line-Start PMSM Operating Performance," *Proc. ICEMS* 2008, 17-20 Oct. 2008, pp.373-378.

[17] D. Stoia, M. Antonoaie, D. Ilea, M. Cernat, "Design of Line Start PM Motors with High Power Factor," Proc. POWERENG 2007, Setubal, Portugal, 12-14 April 2007, published on CD-Rom, IEEE Catalog Number 07EX1654C, ISBN: 1-4244-0895-4, paper 186.

[18] G. Yang, J. Ma, J.X. Shen, and Y. Wang, "Optimal Design and Experimental Verification of a Line-Start Permanent Magnet Synchronous Motor," *Proc. ICEMS* 2008, 17-20 Oct. 2008, pp.:3232 – 3236.

[19] L. Zhiqiang, L. Yingli, L. Xiaofang, Z. Jian, "Pull out Torque Computation for Line Start Permanent Magnet Motor," *Proc. ICEMS* 2008, 17-20 Oct. 2008, pp.3270-3273.

[20] I. Tsuboi, I. Hirotsuka, T. Takegami, and M. Nakamura, "Basic Concept of an Analytical Calculation Method and Some Test Results for Determination of Constant of Line Start Permanent Magnet Motor," *Proc. ICEMS* 2008, 17-20 Oct. 2008, pp. 3108-3111

[21] H.-P. Nee, L. Lefevre, P. Thelin, and J. Soulard, "Determination of *d* and *q* Reactances of Permanent-Magnet Synchronous Motors Without Measurements of the Rotor Position," *IEEE Trans. Ind. Appl*., Vol. 36, No. 5, September/October 2000, pp. 1330-1335.

[22] T. Marcic, G. Stumberger, B. Stumberge, M. Hadziselimovic, and P. Virtic, Determining Parameters of a Line-Start Interior Permanent Magnet Synchronous Motor Model by the Differential Evolution, *IEEE Trans. Magnetics*, Vol. 44, No. 11, Nov. 2008, pp 4385-4388.

[23] A. Levran, E. Levi, "Design of Polyphase Motors with PM excitation," *IEEE Trans. Magnetics*, Vol. 20, No. 3, May 1984, pp. 507-515.

[24] M. Comanescu, A. Keyham, and Min Dai, **"**Design and analysis of 42-V permanent-magnet generator for automotive applications," *IEEE Trans. Energy Conversion*, Vol. 18, Issue 1, March 2003, pp. 107 – 112.

[25] D.C. Hanselman, Brushless Permanent-Magnet Motor Design. New York: McGraw-Hill, 1994.

[26] J.R. Hendershot and T.J. E. Miller, Design of Brushless Permanent-Magnet Motor. Oxford, U.K., Magna Physics/Clarendon, 1994.

[27] T.J.E. Miller, "Brushless Permanent Magnet and Reluctance Motor Drives," Clarendon Press, Oxford, 1989.

[28] D. Stoia, M. Cernat, "Educational Bench of Line-Start Permanent Magnet Synchronous Motors, Part II: The The synchronous operation," *Proc. of the* 4th *Internernational Conf. on Interdisciplinarity in Education ICIE* 2009, Vilnius, 20-21 May 2009.

[29] D. Stoia, M. Cernat, "Educational Bench of Line-Start Permanent Magnet Synchronous Motors, Part III: The The asynchronous operation," *Proc. of the* 4th *International Conf. on Interdisciplinarity in Education ICIE* 2009, Vilnius, 20-21 May 2009.

[30] L. Lefevre, J. Soulard, "Finite element time-transient start of a line-start permanent magnet synchronous motor," *Proc. ICEM*, 2000.

[31] D. Stoia, M. Cernat, "Educational Bench of Line-Start Permanent Magnet Synchronous Motors, Part I: The Operating Point of the Permanent Magnet," *Proc. of the* 4rd *Intern. Conf. on Interdisciplinarity in Education ICIE* 2009*,* Vilnius, 20-21 May 2009

[32] H. Nam, S.B. Park, G.H. Kang, J.P. Hong, J.B. Eom, and T.U. Jung, "Design to Improve Starting Performance of Line-Start Synchronous Reluctance Motor for Household Appliances," *Proc. IEEE IAS Annual Meeting* 2004, pp.79-85.

[33] M. Popescu, T.J.E. Miller, M. McGilp, D.M. Ionel, S.J. Dellinger, "A Unified Approach to the Synchronous Performance Analysis of Single and Poly-Phase Line-Fed Interior Permanent Magnet Motors," *Proc. IEEE IAS Annual Meeting* 2007, 23-27 Sept. 2007, pp. 148 – 153.

[34] Z. Bingyi, Z. Wei, Z. Fuyu, F. Guihong, "Design and Starting Process Analysis of Multipolar Line-Start PMSM," *Proc. ICEMS* 2007, Seoul, 8-11 Oct., 2007, pp. 1629-1634.

[35] B. Zhang, W. Zhang, F. Zhuang, G. Feng, "Design and Starting Process Analysis of Multipolar Line-Start PMSM," Proceeding of International Conference on Electrical Machines and Systems 2007, Oct. 8-11, Seoul, Korea, pp 1629-1634.

[36] T. Miller, "Synchronization of line-start permanent-magnet AC motor," IEEE Trans. Power Apparatus and Systems, vol. PAS-103, July 1984, pp 1822-1828.

[37] T. Miller, "Transient performance of permanent magnet AC machines," *IEEE IAS Annual Meeting* 198 1, Philadelphia, pp. 500-503.

[38] B.L Ahn, W.H. Kim, B.S. Kim, et al., "A Study on the Optimal Barrier Design for High Efficiency of LSPM," *Proc. ICEMS* 2008, 17-20 Oct. 2008, pp. 3427-3429.

[39] A. Nicolaide, Electrical Machines. Scrisul Românesc, Craiova, 1975.

[40] G.E. Chatzarakis, "Nodal Analysis Optimization Based on the Use of Virtual Current Sources: A Powerful New Pedagogical Method," *IEEE Trans. Education*, vol. 52, no. 1, February 2009, pp. 144-150.

[41] D.Ch. Karamousantas, G.E. Chatzarakis, G.N. Korres, P.J. Katsikas, "Obtaining State Equations for Planar Nondegenerate Linear Electric Circuits using Mesh Analysis with Virtual Voltage Sources," *IJEEE* (*International Journal of Electrical Engineering*

Education), Manchester University, Vol. 45, No. 3, July 2008, pp. 239-250.

8. APPENDIX: NOMENCLATURE

B - magnetic flux density;
B_0 - point on the linearized characteristic $B = f(H)$;
b_0 - slot opening;
B_{N0} - magnetic flux density corresponding to the operation point N_0;
B_{rem} - remanent magnetic flux density;
B_{sat} - saturated magnetic flux density;
B_{sy} - yoke magnetic flux density
$B_{\delta\ nonlin}$ - unsaturated magnetic flux density;
$B_{\delta 0}$ - magnetic flux density corresponding to useful air-gap flux $\Phi_{\delta 0}$;
C_p - permeance coefficient;
C_Φ - flux concentration factor;
D_M - mean PM diameter;
f - frequency;
F - magnetomotive force (mmf);
F'_{ad} - rotor referred armature reaction mmf;
F_c - coercive mmf;
F_{ca} - apparent coercive mmf;
F_N - mmf corresponding to the PM operation point N;
F_{rt} - rotor tooth mmf;
F_{ry} - rotor yoke mmf
F_{st} - stator tooth mmf;
F_{sy} - stator yoke mmf;
F_δ - air-gap mmf;
H - magnetic field intensity;
H_c - coercive magnetic field intensity;
H_{ca} - apparent coercive magnetic field intensity;
h_y - yoke height;
H_y - yoke magnetic field intensity;
i - armature current, instantaneous value;
I - armature current, rms value;
k_{ad} - armature reaction factor;
k_C - Carter's coefficient;
k_f - form factor of the excitation field;
k_{fd} - form factor of the armature reaction field;
k_{Fe} - lamination stack coefficient;
k_{sat} - saturation coefficient;
k_w - stator winding factor;
$k_{\sigma M}$ - coefficient of the PM leakage flux;
L - synchronous inductance;
L_{ad} - self inductance;
l_{Fe} - lamination stack length;
L_m - magnetizing inductance;
l_M - PM length in magnetization direction;
l_y - yoke length;
L_σ - leakage inductance;
n_s - synchronous speed;
p - operator p=d/dt; p = j s ω_s ;
p - pole pair number;
P_{em} - rated electromagnetic power;
P_{in} - internal power;
R - stator winding resistance;
R'_D - stator referred damper resistance;
R_D - damper resistance;
s - slip;
S_M - PM cross section area;
S_{sy} - yoke cross section area;
S_δ _ yoke cross section area;
t - tooth width;
T - torque;
T_{av} - average torque;
T_c - cage torque;
T_{em} - electromagnetic torque;
T_l - load torque;
T_{Mbr} - breaking torque;
$T_{p.o.}$ - pull-out torque;
T_{rel} - reluctance torque;
T_{syn} - synchronisation torque;
u - armature voltage, instantaneous value;
U - stator voltage, rms value;
U_e - emf with armature reaction, rms value;
U_{eM} - no-load emf (without arm. reaction), rms value;
$U_{\lim}$ -voltage corresponding to the minimum of the current, rms value;
V_M - PM volume;
w - number of stator windings;
X - synchronous reactance;
X_a - armature reaction reactance;
X_m - magnetizing reactance;
X_σ - leakage reactance;
Z_r - number of rotor slots;
Z_s - number of stator slots;
α_M - pole pitch coverage coefficient of PM;
δ - air-gap length;
ΔP_w - stator winding losses;
θ - internal angle of the synchronous motor;
θ' - angle between $\underline{U}_{eM}$ and $\underline{U}_e$ vectors;
Λ - permeance
Λ_M - PM permeance;
Λ_t - permanence of the external magnetic circuit;
Λ_δ - useful permeance (airgap+teeth+yoke);
Λ_σ - PM leakage permeance;
μ_0 - permeability of vacuum;
μ_{rec} - recoil relative permeability;
τ_p - pole pitch length; τ_s -tooth pitch length;
φ - load angle, between $\underline{U}$ and $\underline{I}$ vectors;
Φ - magnetic flux;
Φ_M - PM magnetic flux;
Φ_N, F_N - coordinates of the operation point N of the PM in flux-mmf coordinates;
Φ_{N0}, F_{N0} - coordinates of the operation point N_0 of the PM in flux-mmf coordinates;
Φ_{rem} - remanent magnetic flux;
Φ_δ - useful air-gap flux with armature reaction;
$\Phi_{\delta 0}$ - useful air-gap flux without armature reaction;
Ψ - flux linked by the stator winding;
ψ - power angle, angle between $\underline{U}_{eM}$ and $\underline{I}$ vectors;
Ψ_a -armature reaction flux linked by the stator winding;
Ψ_D - flux linked by the damper winding;
Ψ_{Mdu} -mutual fluxb etween the PM and the stator winding;
Ω - geometrical synchronous angular speed:
ω_c - cage angular frequency;
Ω_s - angular synchronous speed;
ω_s - synchronous angular frequency;
ξ - saliency ratio.